*Physiol Genomics* 37: 211–224, 2009.
First published March 17, 2009; doi:10.1152/physiolgenomics.90362.2008.

**TRANSLATIONAL PHYSIOLOGY**

# Characterization of a preclinical model of chronic ischemic wound

**Sashwati Roy,[1] Sabyasachi Biswas,[1] Savita Khanna,[1] Gayle Gordillo,[1] Valerie Bergdall,[2] Jeanne Green,[2] Clay B. Marsh,[3] Lisa J. Gould,[4] and Chandan K. Sen[1]**

*Comprehensive Wound Center, Davis Heart and Lung Research Institute, Departments of [1]Surgery, [2]Veterinary Preventive Medicine, and [3]Internal Medicine, The Ohio State University Medical Center, Columbus, Ohio; and [4]Department of Surgery, University of Texas Medical Branch, Galveston, Texas*

Submitted 23 October 2008; accepted in final form 10 March 2009

**Roy S, Biswas S, Khanna S, Gordillo G, Bergdall V, Green J, Marsh CB, Gould LJ, Sen CK.** Characterization of a preclinical model of chronic ischemic wound. *Physiol Genomics* 37: 211–224, 2009. First published March 17, 2009; doi:10.1152/physiolgenomics.90362.2008.— Chronic ischemic wounds presenting at wound clinics are heterogeneous with respect to etiology, age of the wound, and other factors complicating wound healing. In addition, there are ethical challenges associated with collecting repeated biopsies from a patient to develop an understanding of the temporal dynamics of the mechanisms underlying chronic wounds. The need for a preclinical model of ischemic wound is therefore compelling. The porcine model is widely accepted as an excellent preclinical model for human wounds. A full-thickness bipedicle flap approach was adopted to cause skin ischemia. Closure of excisional wounds placed on ischemic tissue was severely impaired resulting in chronic wounds. Histologically, ischemic wounds suffered from impaired re-epithelialization, delayed macrophage recruitment and poorer endothelial cell abundance and organization. Compared with the pair-matched nonischemic wound, unique aspects of the ischemic wound biology were examined on *days 3, 7, 14,* and *28* by systematic screening of the wound tissue transcriptome using high-density porcine GeneChips. Ischemia markedly potentiated the expression of arginase-1, a cytosolic enzyme that metabolizes the precursor of nitric oxide L-arginine. Ischemia also induced the SOD2 in the wound tissue perhaps as survival response of the challenged tissue. Human chronic wounds also demonstrated elevated expression of SOD2 and arginase-1. This study provides a thorough database that may serve as a valuable reference tool to develop novel hypotheses aiming to elucidate the biology of ischemic chronic wounds in a preclinical setting.

oxygen; porcine; swine; microarray

THE PUBLIC HEALTH IMPACT OF chronic wounds is staggering. An estimated 1.3 million to 3 million US individuals are believed to have pressure ulcers; and as many as 10–15% of the 20 million individuals with diabetes are at risk of developing chronic ulcers. Many more have venous ulcers or wounds that result from arterial disease. Treating these wounds costs an estimated $5 billion to $10 billion each year (33). Animal wound healing models are important biological tools to understand basic processes of tissue repair and to develop and validate strategies for clinical treatment. Over the years, basic and clinical research has revealed much about the individual molecular and cellular processes involved in wound healing, but attempts to accelerate and/or improve wound healing by enhancing, inhibiting, or modifying isolated aspects of the wound healing process have met with only limited success. According to the National Institute of General Medical Sciences, a major sponsor of wound healing research in the United States, research to advance wound care is handicapped by the limitations of animal model systems in mimicking human wound healing (http://grants.nih.gov/grants/guide/rfa-files/RFA-GM-06-002.html) (50). Although small mammals such as the mouse, rat, rabbit, and guinea pig are frequently used in wound healing studies, relevance of such models to the human wound is questionable. These small mammals have several anatomical and physiological characteristics that are in sharp contrast with the human skin. Examples include a dense layer of body hair and thin epidermis and dermis, and most importantly these small mammals close their wounds primarily through contraction as opposed to re-epithelialization noted in humans. It is therefore not surprising that results from such small mammal studies show only 53% concordance with human studies. In contrast, wound healing studies in pigs show a striking 78% concordance with human studies (58). Anatomically as well as physiologically, pig skin closely resembles human skin (40, 58). Pig skin and human skin share similar patterns of hair follicles and blood vessels. Biochemically, pig skin contains dermal collagen and has a dermal elastic content that is more similar to humans than other commonly used mammals (23). Additionally, pigs and humans have similar physical and molecular responses to various growth factors (5). The porcine model is thus generally accepted as an excellent tool to study wound healing (4, 40, 54, 58, 63, 64).

Vascular complications commonly associated with problematic wounds are primarily responsible for wound ischemia. Ischemia limits the supply of blood-borne products, including nutrients, oxygen, and circulating cells, to the wound site, thereby severely impairing the healing response (41, 51). Development of mechanism-based understanding of the ischemic wounds in humans is limited by a number of complicating factors. First, most humans suffering from an ischemic wound also suffer from several other comorbid conditions that make research design to address a pointed hypothesis highly challenging. Second, chronic ischemic wounds presenting at wound clinics are heterogeneous with respect to etiology, age of the wound, and other factors complicating wound healing. In addition, there are ethical challenges associated with collecting repeated biopsies from a patient to develop an understanding of the temporal dynamics of the mechanisms underlying chronic wounds. Taken together, while the study of ischemic wounds in a clinical setting is highly valuable, the need for a preclinical

Address for reprint requests and other correspondence: C. K. Sen, 512 Davis Heart & Lung Research Inst., 473 W. 12th Ave., Ohio State Univ. Medical Center, Columbus, OH 43210 (e-mail: chandan.sen@osumc.edu).

model of ischemic wound is compelling. Given the unique advantages of the porcine model to study wound healing as a preclinical approach, we sought to develop and characterize the first porcine model of ischemic wound utilizing current imaging as well as functional genomic technologies.

## MATERIAL AND METHODS

### *Porcine Ischemic Excisional Wound Model*

A total of 20 ($n = 4 \times 5$ time points, see Fig. 7) domestic white pigs were used in this study. All experiments were approved by the Ohio State University Institutional Laboratory Animal Care and Use Committee (ILACUC). Pigs (70–80 lb) were anesthetized with Telazol followed by isoflurane. The dorsal region was shaved. The skin was surgically prepared with alternating Betadine and alcohol scrubs. Under such aseptic conditions, four full-thickness bipedicle skin flaps measuring 15 × 5 cm were developed on each animal by means of parallel incisions as shown in Fig. 1. The incisions were made using electrocautery. The dermal flap was elevated from the underlying subcutaneous tissue. Precut (same as that of the dimensions of the flap), sterilized 0.01-inch-thick Sil-Tec medical-grade sheeting (Technical Products Inc. of Georgia, Decatur, GA) was then placed underneath the flap to prevent readherence and reperfusion of the flap from the underlying tissue (18). The skin flap incisions and silicon sheet were sutured into position using 3-O Ethilon continuous sutures. Ischemia of the flap tissue was verified by laser Doppler imaging (Fig. 2) of blood flow.

### *Wounding*

Full-thickness excisional wounds were developed in the middle of each flap using a 8 mm disposable biopsy punch. Six more wounds were developed similarly on nonischemic skin (Fig. 1). The flap incisions were dressed with VAC Drape (KCI). The dressing was changed every 3 days, and any accumulating wound fluid was drained as needed. The ischemic and nonischemic wounds were digitally imaged for collection of wound closure data. On designated time points, the entire wound tissue (1.5 × 1.5 cm with the 8 mm wound at the center) was harvested for tissue analyses (RNA, protein, and histological analyses). After the completion of experiments, pigs were either euthanized or transferred to another ILACUC-approved protocol.

*Determination of wound area.* Imaging of wounds was performed with a digital camera (Canon PowerShot G6). The wound area was determined using WoundMatrix software as described previously (52).

### *Skin Perfusion Pressure*

Skin perfusion pressure (SPP) (67) was measured using a Sensi-Lase system (Väsamed, Eden Prairie, MN). The test measures skin perfusion with a laser Doppler sensor assembly (LSA) located beneath a pressure cuff for application and release of pressure to limb or specified area. During the measurement, the pressure cuff is automatically inflated until the LSA determines that perfusion beneath the cuff has stopped. The pressure is then automatically released at a controlled rate while the cuff pressure and skin perfusion pressure are measured. A graph displays pressure and perfusion during cuff deflation and indicates the pressure at which the skin perfusion resumes (Fig. 1, *C* and *D*).

### *Laser Doppler Blood Flow Imaging*

The MoorLDI-Mark 2 laser Doppler blood perfusion imager (resolution: 256 × 256 pixels in the region of interest; each pixel being an

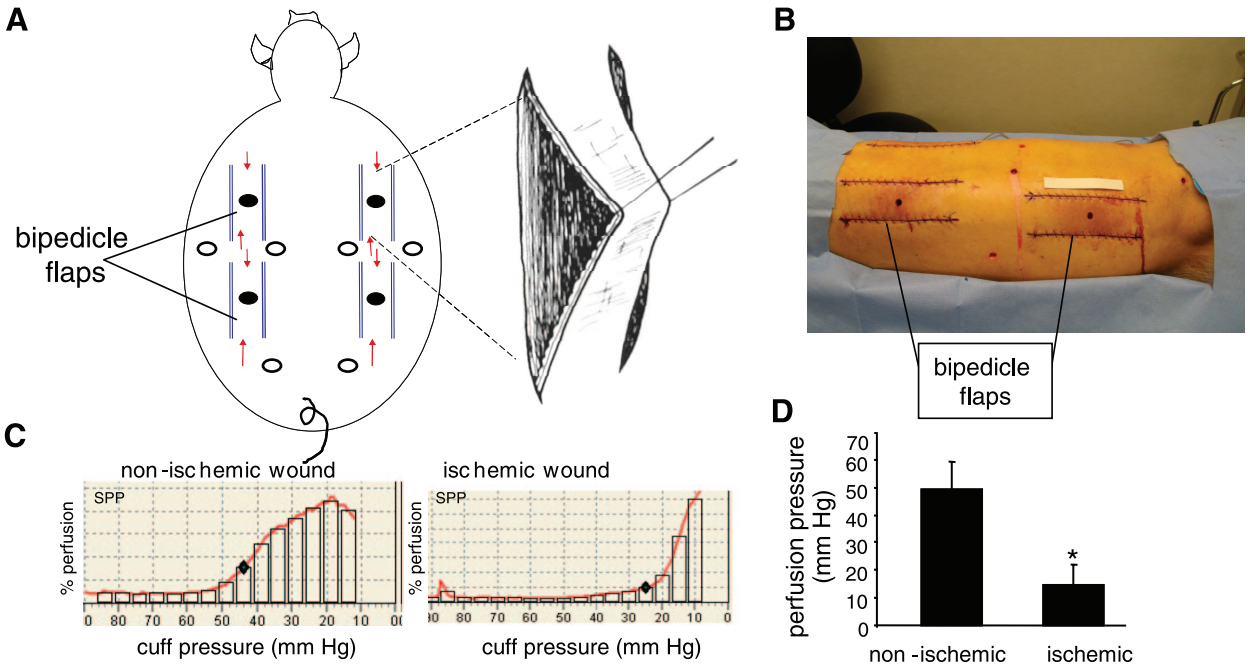


Fig. 1. Wounding approach and skin perfusion pressure. *A, B*: 4 bipedicle flaps (15 × 5 cm) were developed on the back of domestic white swine. The flaps were freed from the underlying muscle and a sterile silicone sheet (15 × 5 cm) was placed under it to prevent readherence. The incised edges of the flap were sutured to the adjacent skin incorporating the silicone. Full-thickness excisional wounds were developed in the middle of each flap (filled circles) using a 8 mm disposable biopsy punch. Six additional paired wounds were developed similarly in the adjacent nonischemic skin (open circles). Arrows in *A* indicate direction of blood flow. Scale: the paper strip above the left lumbar flap in *B* is 10 cm long. *C*: skin perfusion pressure (SPP) was measured at locations adjacent to the ischemic as well as paired nonischemic wounds. ◆, The cuff pressure where subcutaneous microcirculation was restored. *D*: SPP from nonischemic and ischemic wounds. Data are means ± SD ($n = 3$); *$P < 0.01$.

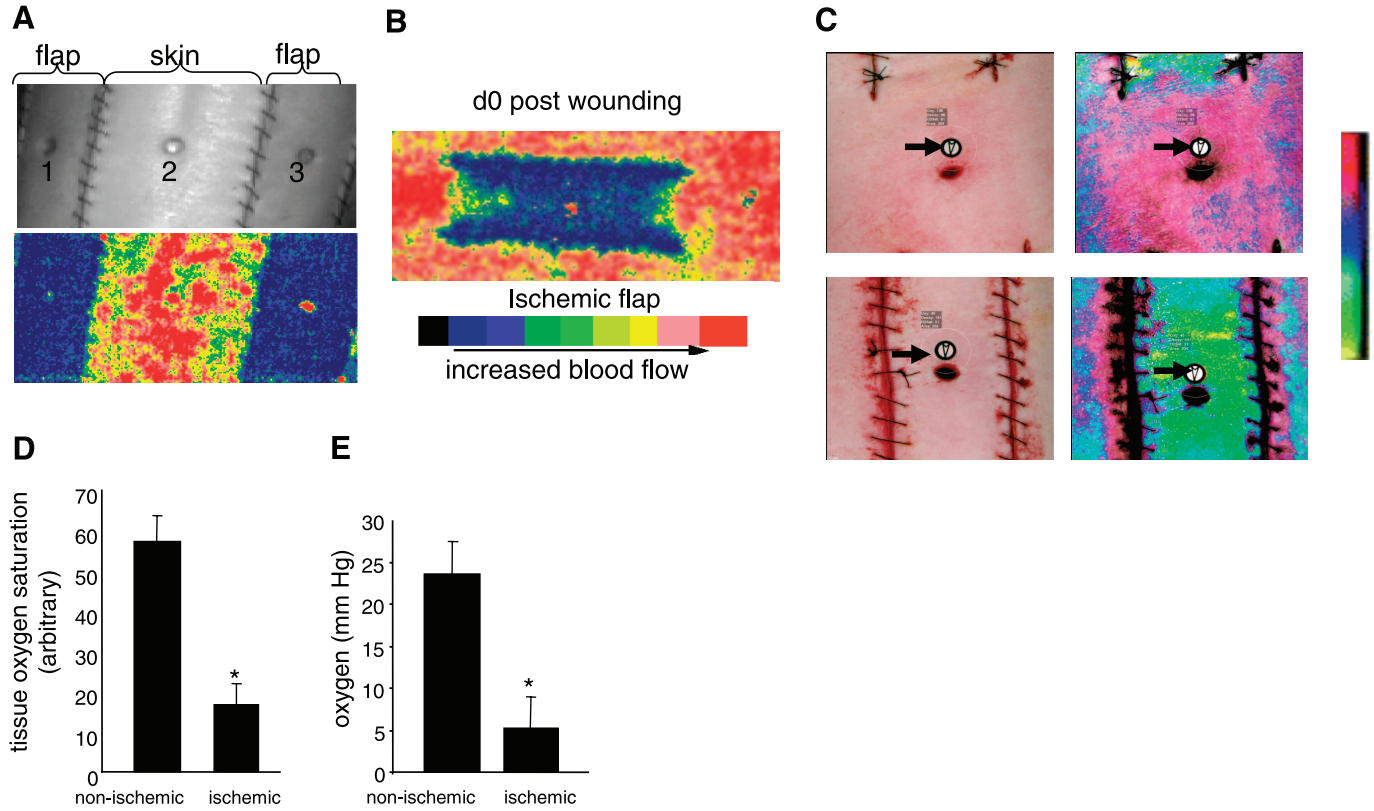


Fig. 2. Characterization of wound-site ischemia and hypoxia. *A*: photographic (*top*) and Doppler (*bottom*) images of the back of swine with ischemic flaps and skin with intact perfusion. Nonischemic (2) and ischemic wound (1, 3) locations are marked; *B*: laser Doppler image of an ischemic flap on *day 0* postwounding. *C*: wound tissue oxygen saturation and oximetry performed using a hyperspectral scanner (*C, D*) or OxyLite (*E*). *C*: representative photographic (*left*) and corresponding hyperspectral images (*right*) from nonischemic (*top*) and ischemic (*bottom*) wounds captured using a OxyVu2 hyperscpectral imaging system. The white circle and black arrows represent the hyperspectral target used for imaging. *D*: quantification of tissue oxygen saturation values from nonischemic and ischemic wounds as shown in *C*. Data are means ± SD ($n = 4$); $^*P < 0.01$. *E*: wound-bed tissue $Po_2$ was measured using OxyLite based on fluorescence quenching principle. d, Day. Data are means ± SD ($n = 4$), $^*P < 0.05$.

actual measurement) employs a visible red laser beam (633 nm) to map tissue blood flow and enable quantification (Fig. 2*A*).

*Hyperspectral Imaging*

Medical hyperspectral imaging is a novel noninvasive technique that utilizes visible light for the spectral analyses of tissue oxyhemoglobin and deoxyhemoglobin and calculates the oxygen saturation based on their relative abundance (6, 30, 56). Hyperspectral imaging was performed using OxyVu-2 system (Hypermed, Burlington, MA) according to the manufacturer's instructions.

*Tissue Partial Pressure of Oxygen Determination*

Tissue $Po_2$ measurements were estimated on the basis of fluorescence quenching using the OxyLite tissue oximetry device (Oxford Optronics, Oxford, UK) and by applying a needle (23 G) encased oxygen sensor as described previously (13).

*Histology*

Formalin-fixed paraffin-embedded or OCT-embedded frozen wound-edge specimens were sectioned. The paraffin sections were deparaffinized and stained with hematoxylin and eosin and Masson's Trichrome staining by standard procedures. Immunohistochemical staining of paraffin or frozen sections was performed as described earlier (46) using the following primary antibodies: anti-macrophage, L1 calprotectin (1:200; MAC387; Neomarker, Fremont, CA); K14 (1:100; Covance, Emeryville, CA); von Willebrand factor (vWF, 1:200; Dako Cytomation, Carpinteria, CA); anti-arginase 1 (1:100, BD Biosciences, San Jose); and anti-superoxide dismutase 2 (SOD2, 1:100; Abcam, Cambridge) after heat-induced epitope retrieval where necessary. Secondary antibody detection and counterstaining were performed as described previously (46). The area of stain was quantitated with Adobe Photoshop 6.0 by a color subtractive process (62). We determined re-epithelialization from Masson's trichrome-stained images by measuring the original width of the wound (W) and then measuring the portions of the wound that had re-epithelialized (E). Percent-repithelialized was calculated as: (E/W) × 100.

*GeneChip Probe Array Analyses*

To identify clusters of transcripts differentially expressed during the temporal course of healing, the GeneChip high-density microarray approach was adopted (45–50). Total RNA was extracted (TRIzol, GIBCO-BRL) from wound tissue on 0, 3, 7, 14, and 28 (postheal tissue in the case of closed wounds) days after wounding. Further clean-up of RNA was performed using the RNeasy kit (Qiagen). The quality of RNA thus obtained was examined using the Agilent 2100 Bioanalyzer. Targets were prepared for microarray hybridization according to previously described protocols (45–50). To assess the quality of hybridization, samples were hybridized for 16 h at 45°C to GeneChip test arrays. Satisfactory samples were hybridized with the GeneChip Porcine Genome Array (Affymetrix) for the screening of over 24,000 probe sets. The arrays were washed, stained with streptavidin-phycoerythrin, and were then scanned with the GeneArray scanner (Affymetrix) in our own facilities as described earlier (45–

50). Data were collected from four pigs ($n = 4$) in each time point for paired nonischemic and ischemic wound samples (Fig. 7).

*Data analyses.* Data acquisition and image processing were performed using Gene Chip Operating Software (Affymetrix). Raw data were collected and analyzed using a Stratagene ArrayAssist Expression Software v. 5.1 (Stratagene). Additional processing of data was performed using dChip software (v. 1.3, Harvard University) (46, 50). GC-RMA was applied for data normalization. Differentially expressed genes were identified using a two-class *t*-test where significance level was set at $P < 0.05$ with Benjamin-Hochberg correction for false discovery rate (45–50). All wound-responsive genes that were significantly changed ($P < 0.05$ with Benjamin-Hochberg correction) at any single time point compared with 0 h prewound skin samples were subjected to hierarchical clustering (Fig. 8, *A* and *B*). Major clusters of genes that changed during the course of healing were identified. The genes from the cluster were subjected to functional analysis using DAVID [Database for Annotation, Visualization and Integrated Discovery; National Institute of Allergy and Infectious Diseases, National Institutes of Health (NIH)] and gene ontology. To study wound-responsive genes that were differentially expressed in ischemic wounds compared with paired nonischemic wounds at any given time point, hierarchical clustering and subclustering were performed (Fig. 9 and Supplemental Table S1[1]). Select, differentially expressed candidate genes were verified by quantitative real-time PCR (Fig. 10). Cell-specific sources of genes listed in Supplemental Table S3 are listed with references in Supplemental Table S2.

### *Reverse Transcription and Quantitative Real-time PCR*

Tissue mRNA was quantified by real-time or quantitative (Q) PCR assay using the double-stranded DNA binding dye SYBR Green-I as described previously (45–50). The primer set used for the individual genes are listed below. β-Actin was used as a reference housekeeping gene.

Pig_PON3 F: 5′-GGGGCAGGATGCCATCCTAAT-3′, Pig_PON3 R: 5′-CAGAGCTGCCCTGAAGCACAG-3′, Pig_SOD2 F: 5′-GCAGCTCGAGCAGGAATCTGG -3′, Pig_SOD2 R: 5′-TTGTTCACGTAGGCCGCGT-3′, Pig_TIMP1 F: 5′-CAAGCGTTATGAGATCAAGATGACC-3′, Pig_TIMP1 R: 5′-TCCACAGTTGTCCAGCTATGAGAA-3′, Pig_MCP-1 F: 5′-CAGTAAGAAGATCTCGATGCAGCG-3′,Pig_MCP-1 R: 5′-TTCTTGTCCAGGTGGCTTATGG-3′, Pig_IL8 (AMCF1) F: 5′-CCTGCTTTCTGCAGCTCTCTGTGA-3′, Pig_IL8 (AMCF1) R: 5′-GTACAACCTTCTGCACCCACTTTT-3′, Pig_IGF1 F: 5′-CACAGGGTACGGCTCCAGCA-3′, Pig_IGF1 R: 5′-TTGGGCATGTCCGTGTGGC-3′; Human_SOD2 F: 5′-GGTATCTGGGCTCCAGGCAGAA-3′, Human_SOD2 R: 5′-TGGGTTCTCCACCACCGTTA-3′, Human_ARG1 F: 5′-AGTATTGAGAAAGGCTGGTCTGCTT-3′, Human_ARG1 R: 5′-CGTTCTTCTTGACTTCTGCCACCTT-3′.

### *Human Subjects*

Subjects with chronic wounds were recruited from the Ohio State University Comprehensive Wound Center outpatients' clinics as described (50). Skin samples were obtained from individuals without any chronic wounds. Protocols were approved by the Ohio State University's Institutional Review Board. Wound-edge skin (50) (at the wound perimeter) or intact skin biopsies (3 mm) were obtained from individual subjects and immediately frozen in liquid nitrogen until further analysis.

### *Statistics*

Results are presented as means ± SD. Difference between means was tested by Student's *t*-test or ANOVA as appropriate. A value of $P < 0.05$ was considered statistically significant. Microarray data processing is described above under *GeneChip Probe Array Analyses*.

[1] The online version of this article contains supplemental material.

## RESULTS

Survival of skin flaps is known to depend on their dimension, which in turn determines the graded levels of ischemia throughout the flap tissue (18, 27, 28). We chose to force skin ischemia by adopting a full-thickness bipedicle flap approach as shown in Fig. 1*A*. The goal was to generate an ischemic piece of skin tissue that would survive over a period of at least 4–6 wk. First, we focused on optimizing the dimensions of the flap (20). Initially, we observed that the bipedicle flaps were very aggressive in recruiting blood supply from the underlying muscle tissue (not shown). Such response was in conflict with our intent to maintain ischemia in the raised skin tissue over weeks. We addressed this by choosing to insert a sterile silicone sheet between the skin and the muscle. Suturing of the skin flap incision was performed such that the silicon sheet was included in the sutured skin edges. This measure helped maintain long-term flap ischemia, as intended. Our efforts to identify the appropriate dimensions of the flap led to the observation that for bipedicle flaps in pigs, a length/breadth ratio of 3:1 results in long-term ischemia in surviving flaps. We selected 15 cm length and 5 cm breadth as the final dimension because this helped us place four such flaps on the back of each adult pig (Fig. 1*A*). Among a number of noninvasive diagnostic methods, measurement of the SPP has proven utility for assessing the severity of ischemia at the wound site. Measurement of SPP represents an objective approach to assess the severity of peripheral arterial disease or for predicting wound healing (53, 67). SPP measurements from the above-described bipedicle flaps and comparison with SPP measured from the adjacent intact skin demonstrated that the bipedicle flaps had an SPP consistent with the SPP of chronic nonhealing wounds (Fig. 1, *C* and *D*). The pair-matched SPP recorded in the intact pig skin tightly matched the values seen in healing wounds (67). Full-thickness biopsy wounds were placed on the ischemic tissue or adjacent nonischemic tissue as shown in Fig. 1, *A* and *B*.

Further characterization of the state of tissue ischemia was performed by applying three additional technologies: laser Doppler imaging, hyperspectral scanning, and tissue oximetry (Fig. 2). Laser Doppler imaging is an useful technique for measuring microvascular perfusion in wounds because it involves no contact and produces a color image representing flow distribution over an area of tissue (29). Close-up images shown in Fig. 2*A* demonstrate a clear contrast in blood flow between the flap and adjacent intact skin. The flaps on both sides are markedly ischemic compared with the intact skin separating the two flaps (Fig. 2*A*). Laser Doppler image of the entire flap demonstrates lack of blood supply to the flap from the incisional edges and graded ischemia in the flap with the centre (wound site) being the most ischemic (Fig. 2*B*). Hyperspectral scanning technology has recently emerged as being productive in characterizing tissue ischemia by noninvasively monitoring tissue oxyhemoglobin and deoxyhemoglobin ratio (30). It has enabled the detection of early changes in the skin microcirculation in patients (19). The hypoxia component of tissue ischemia was characterized by hyperspectral scanning (Fig. 2*C*). Compared with the intact skin, the flaps clearly suffered from hypoxic challenge as illustrated in Fig. 2*C*. Quantitative analyses of the images demonstrated that the tissue oxygen saturation at the ischemic wound site was one-third of the values collected from the adjacent intact skin (Fig. 2*D*). Direct

measurement of tissue oxygen tension utilizing an oximetry approach provided consistent results (Fig. 2*E*). The oxygen tension at the ischemic wound site closely matched the values reported from ischemic wounds in patients. Clinically, in nondiabetics chronic wounds are known to result when the wound site $P_{O_2}$ value is <10 mmHg (2, 12, 22). Consistently, in our model we noted that the closure of ischemic wounds with $P_{O_2}$ <10 mmHg were significantly impaired (Fig. 3*A*), resulting in chronic wounds that did not close in 30 days (Fig. 3*B*).

Pair-matched histological characterization of the wound healing biology resulted in the observation that ischemic wounds suffered from impaired re-epithelialization (Fig. 4). Wound-edge tissue, as demarcated by open boxes in Fig. 4*A*, were stained for keratin-14, the type I cytokeratin that forms the cytoskeleton of epithelial cells. While the nonischemic healing wound showed clear presence of the anticipated hyperproliferative epithelium, development of a hyperproliferative epithelium was severely compromised in the pair-matched ischemic wounds (Fig. 4, *B* and *C*).

The macrophages in the tissue sections were detected using antibody against leukocyte L1 protein. In porcine tissue, this antibody has been reported as reliable marker for infiltrating macrophages (8). The antigen also known as calprotectin, a myelomonocytic protein, has been also shown to be expressed by neutrophils (24). Infiltration of macrophages into the wound site represents a key component of the acute inflammatory phase of wound healing (46). Macrophage infiltration was rapid in nonischemic wounds with a peak at 3 days postwounding. The number of macrophages at these wound sites decreased on *day 7* postwounding (Fig. 5). In contrast, pair-matched ischemic wounds drew in macrophages very slowly, resulting in a delayed inflammatory phase (Fig. 5). Such observation was associated with the finding that ischemic wounds suffered from impaired vascular development. vWF is a large multimeric glycoprotein produced constitutively in the endothelium. On *day 7* postwounding, nonischemic wounds displayed organized $vWF^+$ cellular structures indicative of vascular formation. These structures were much more prominently displayed on *day 14* postwounding (Fig. 6). In sharp contrast, wound tissue from pair-matched ischemic wounds showed scattered and disorganized presence of endothelial cells suggestive of impaired vascular formation (Fig. 6).

The microarray study and data analysis design is illustrated in Fig. 7 and was modeled on the basis of our previously published studies (45, 46, 48, 50). A total of 24,124 probe sets were utilized to comprehensively screen the porcine transcriptome. Pair-matched nonischemic and ischemic wounds were examined in five different time points (Fig. 7). Subcluster analyses were performed to identify wound-responsive genes at any given time point. Next, further data mining was performed to identify the list of wound-responsive genes at any given time point that were also sensitive to ischemia. Results illustrated at the bottom of Fig. 7 show that compared with the transcriptome of the intact skin on *day 3*, the expression of 930 transcripts changed in response to wounding. Fifty-six of these 930 transcripts (i.e., 6%) were sensitive to ischemia. On *day 7*, the number of transcripts whose expression changed in response to wounding sharply raised to 1,956, roughly twice the corresponding number on *day 3*. Roughly 5% of these wound-responsive genes were sensitive to ischemia on *day 7*. On *day 14*, only 960 wound-responsive transcripts were detected. Of these, just over 15% of the transcripts were sensitive to ischemia. On *day 28*, the total number of wound-responsive genes detected was 987. Of these, ~4% of the transcripts were sensitive to ischemia (Fig. 7). To further mine the data, the focus was first set on the temporal study of nonischemic wounds (Fig. 8, Supplemental Table S1). Hierarchical cluster analyses identified six major clusters of transcripts (Fig. 8*A*, *a–f*) that were upregulated. Transcripts belonging to each cluster are listed in Supplemental Table S1, *a–f*. All the transcripts that were downregulated in response to wounding clustered into one set as shown in Fig. 8*B* (Supplemental Table S1*g*). Next, we sought to analyze the wound-responsive genes that were sensitive to ischemia (Fig. 9). On *days 3, 7,* and *14*, wound-responsive ischemia-sensitive transcripts fell into two clusters for each day. On *day 28*, wound-responsive ischemia-sensitive transcripts fell under three different clusters (Fig. 9, *g*, *h,* and *i*). A complete list of genes represented by these nine clusters over four different time points after wounding is presented in Supplemental Table S3. To test the robustness of our microarray analyses, select candidate genes identified by

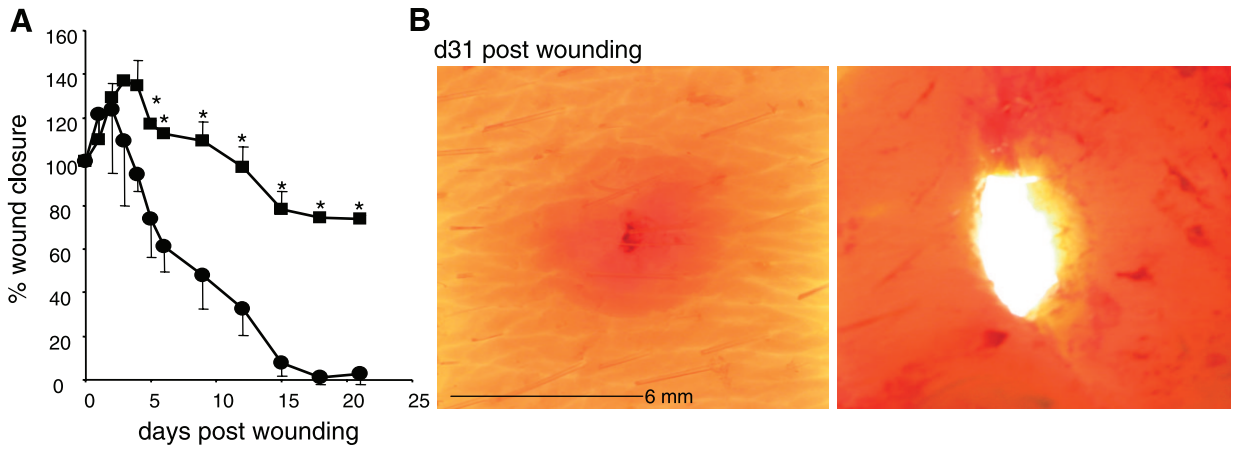


Fig. 3. Impaired wound closure in ischemic wounds. *A*: closure in nonischemic (●) and paired ischemic (■) wounds. Data are shown as percentage of the initial wound area. Data are means ± SD ($n = 4$). *$P < 0.05$ compared with time zero postwounding. *B*: images of skin containing nonischemic (*left*) and paired ischemic (*right*) wound 31 days after wounding.

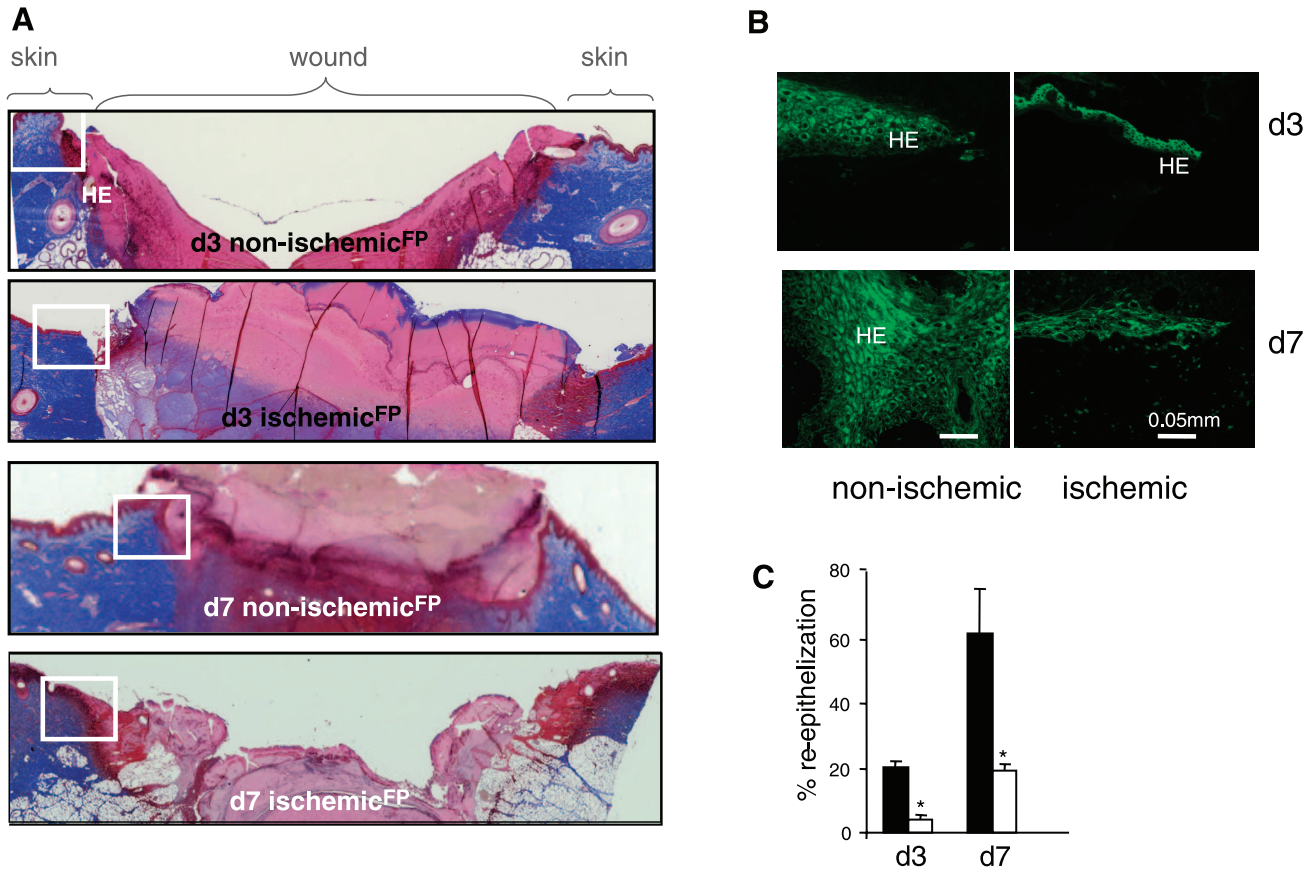


Fig. 4. Impaired re-epithelialization of ischemic wounds. Wound-edge tissues were collected at the indicated time points after wounding. Formalin-fixed paraffin-embedded wound biopsies were sectioned (5 μm) and stained using the following approaches: *A*: Masson's trichrome procedure. This results in blue-black nuclei and blue collagen and cytoplasm. Epidermal cells appear reddish. Mosaic images showing nonischemic and ischemic wounds on *days 3* and *7* after wounding. The mosaic images of whole wounds were collected under ×20 magnification guided by MosaiX software (Zeiss) and a motorized stage. Each mosaic image was generated by combining 12–15 images. Boxed area marks the wound-edge region of the tissue shown in *B*. HE, hyperproliferative epithelium; FP, fibrin plug. *B*: keratin 14 (K14) immunofluorescence staining. K14 (green) is known to specifically stain keratinocytes (basal layer). Marked impairment of re-epithelialization was noted in ischemic wounds in both *days 3* and *7* postwounding compared with corresponding non ischemic wounds. *C*: quantitation of re-epithelialization in Mason trichrome stained ischemic and nonischemic wounds on *days 3* and *7* postwounding. Re-epithelialization was determined by measuring the original width of the wound (W) and then measuring the portions of the wound that had re-epithelialized (E). Using the re-epithelialized area as the numerator and the original width as the denominator and multiplying by 100 gives the percentage of the wound re-epithelialized (E/W) × 100 = percent re-epithelialization. Data are means ± SD ($n = 3$); *$P < 0.05$.

the microarray approach were validated by QPCR. Results of the microarray study were observed to be in tight agreement with findings from the quantitative assay of single candidate genes (Fig. 10). Wounding was noted to markedly induce the expression of arginase-1 (Fig. 9, cluster *a*; Supplemental Table S3*A*), a cytosolic enzyme that catalyzes the fifth and final step in the urea cycle, converting L-arginine into L-ornithine and urea. L-arginine is a key substrate for the synthesis of the major vasoregulatory signaling molecule, nitric oxide (10, 69). Wound-responsive induction of arginase-1 gene expression was markedly enhanced in ischemic wounds. Immunohistochemical staining of the wound tissue sections consistently demonstrated that indeed ischemic wound tissue possesses a higher abundance of Arg-1 (Fig. 11, *A–C*). Consistent with findings in our porcine model of chronic wound, elevated expression of SOD2 as well as Arg-1 was noted in human chronic wound tissue (Fig. 11, *G* and *H*). Colocalization studies with porcine tissue recognized endothelial cells at the wound site as one of cell type expressing Arg-1 (Fig. 12). SOD2 or mitochondrial SOD is known to be markedly induced in response to oxidative stress (66). Akin to Arg-1, wounding induced SOD2 and such gene expression was markedly higher in ischemic wounds, perhaps as a survival response of the challenged tissue. Immunohistochemical assay for SOD2 demonstrated a significantly higher abundance of SOD2 in the ischemic wound tissue compared with that in pair-matched nonischemic wound tissue (Fig. 11, *D–F*). Taken together, results from the QPCR as well as immunohistochemical studies effectively validate the microarray analyses performed in this study.

## DISCUSSION

Ischemic wounds are known to be associated with great loss of both limb and life (43, 55). Thus, clinically presented ischemic wounds do not readily lend themselves to the study of biological mechanisms because the collection of tissue biopsies at multiple time points from the same wound poses ethical challenges. The need for preclinical models of ischemic wounds is therefore compelling. Skin flaps represent a proven

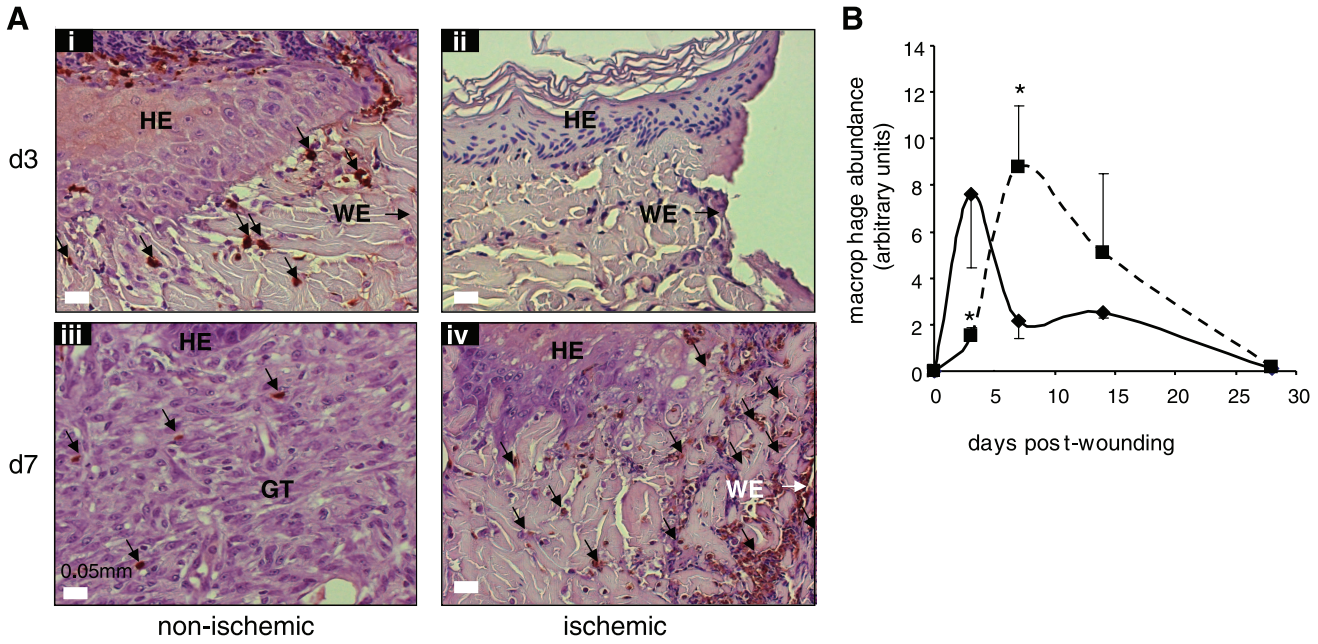


Fig. 5. Dysregulated macrophage infiltration in ischemic wounds. Wound-edge tissues were collected at the indicated time points after wounding. Formalin-fixed paraffin-embedded biopsy tissues were sectioned (5 μm) and stained using L1 macrophage/calprotectin immunostaining (brown). *A*: representative images of ischemic (*right*) and nonischemic (*left*) wounds showing macrophages (brown). The tissue sections were counterstained with hematoxylin (blue). HE, hyperproliferative epithelium; GT, granulation tissue; WE, wound-edge orientation; *B*: kinetics of macrophage infiltration in the nonischemic (solid line, ◆) and ischemic wounds (dotted line, ■). Relative quantification (arbitrary units) of macrophages in the tissue sections obtained 3–28 days postwounding was performed using an image processing tool kit. Data are means ± SD ($n = 3$). *$P < 0.05$.

classical approach to induce ischemia (14, 27, 28, 37, 60). In this study, the flap dimensions were optimized such that the tissue was ischemic but not necrotic. Such approach enabled the pair-matched long-term study of a full-thickness wound placed at the most ischemic site of the skin tissue compared with a similar wound placed on the adjacent perfused skin of the same pig. Ischemia is defined by lowered blood supply to the tissue and therefore compromised microcirculation. Limitations in the ability of the vasculature to deliver $O_2$-rich blood to the wound tissue leads to, among other consequences, hypoxia. Tissue hypoxia reflects a reduction in oxygen delivery below tissue demand, whereas ischemia is a lack of perfusion, characterized not only by hypoxia but also by insufficient supply of other blood-borne products including nutrients (51). In this study, the ischemic wounds had significantly lower blood flow as measured by laser Doppler imaging. SPP, a measure of

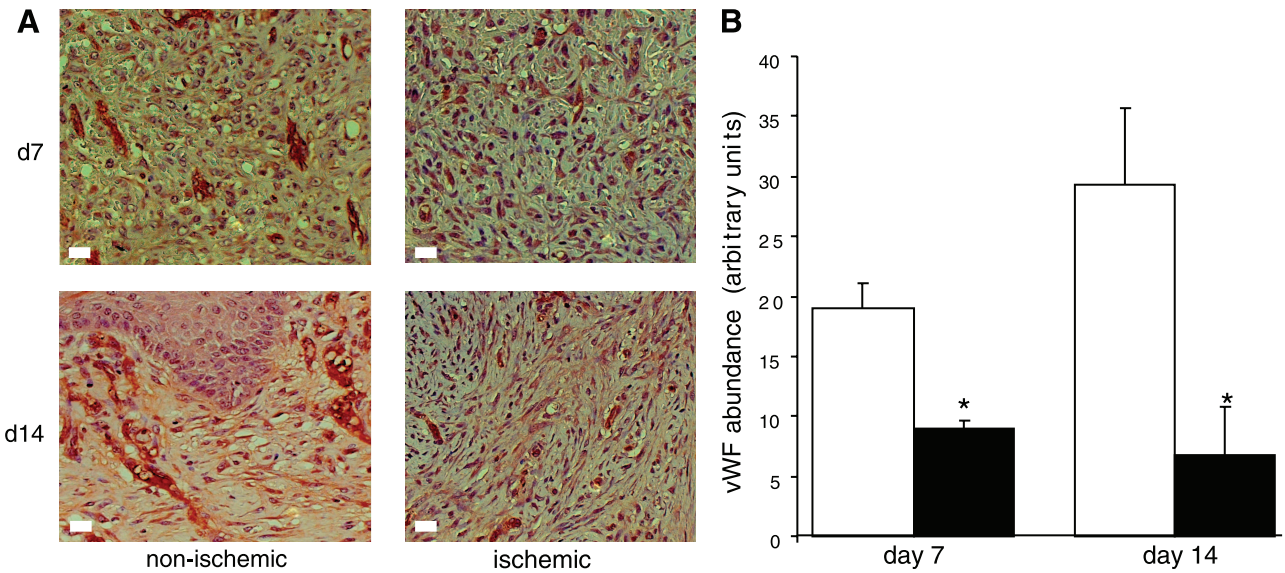


Fig. 6. Endothelial cell abundance is limited in ischemic wounds. Wound-edge tissues were collected at the indicated time points after wounding. Formalin-fixed paraffin-embedded biopsy tissues were sectioned (5 μm) and stained using von Willebrand Factor (brown) and counterstained with hematoxylin (blue). Compared with nonischemic wounds, ischemic wounds showed fewer organized endothelial cell clusters (*A*). In addition, endothelial cell abundance was poorer in the ischemic wounds (solid bars) compared with nonischemic (open bars) at both time points studied (*B*). Data are means ± SD ($n = 3$). *$P < 0.05$.

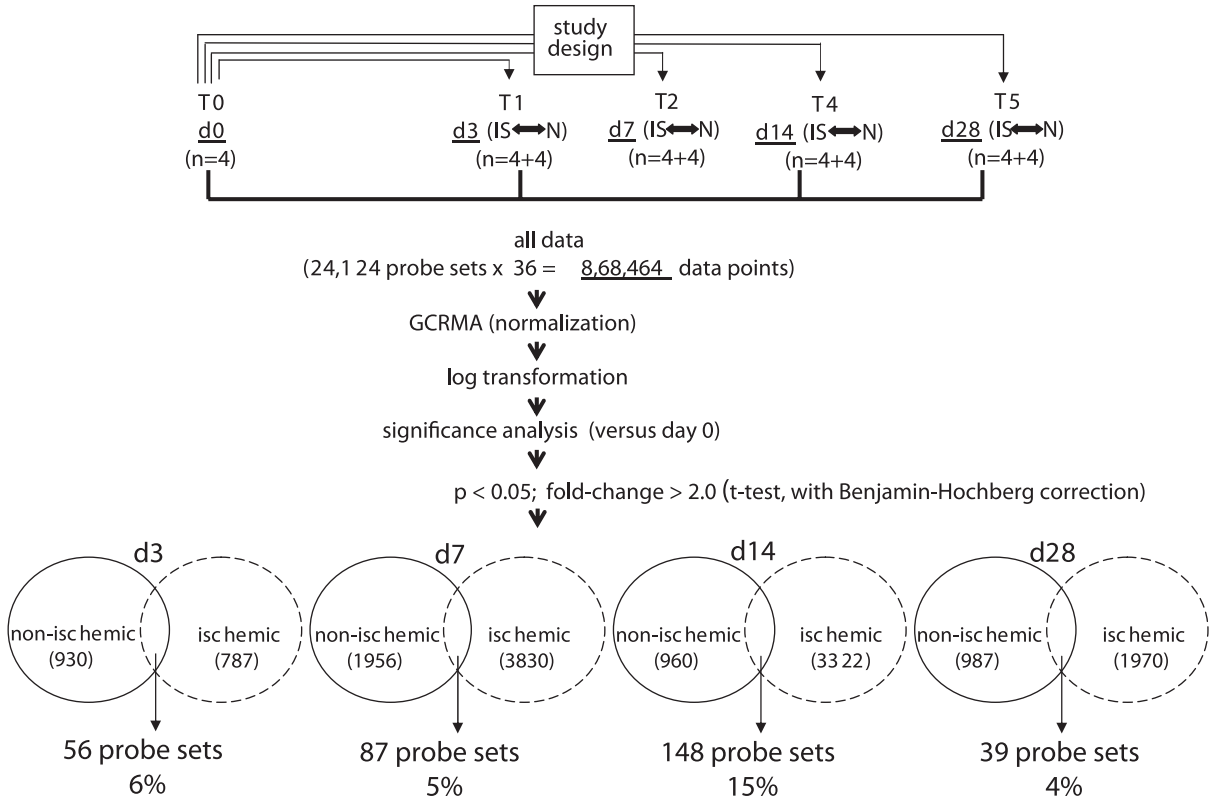


Fig. 7. GeneChip data analysis scheme used to identify the kinetics of differentially expressed genes in nonischemic and ischemic wounds. Image acquisition and processing was performed using GCOS (GeneChip operating software, Affymetrix). GC-RMA was applied for data normalization. ArrayAssist v. 5.1 software was used to identify significant ($P < 0.05$; false discovery rate corrected) differentially expressed genes in nonischemic wound tissue compared with skin (0 h). The list of wound-sensitive genes thus obtained was queried for differential expression under ischemic vs. nonischemic conditions. The numbers of such wound-responsive ischemia-sensitive transcripts are indicated at the bottom together with a percentage value that represents the fraction of the total number of wound-responsive transcripts that were ischemia-sensitive for the corresponding time point after wounding.

microcirculation and a proposed predictor of wound healing (53, 67), was significantly compromised in the ischemic wounds. Consistently, the ischemic wounds were hypoxic. The extent of hypoxia was comparable to that noted in problematic ischemic wounds presented clinically (2, 12, 22). The Center for Medicare and Medicaid Services of the United States Department of Health and Human Services defines chronic wounds as nonhealing cutaneous wounds that persist for 30 days or longer and fail to properly complete the healing process (7). Wound closure in the ischemic pig skin tissue was severely impaired, resulting in wounds that persisted for 30 days or longer. The developed model, therefore, provides an opportunity to understand the biology of chronic wounds in a preclinical setting.

Wound closure is the single-most important outcome as viewed by the United States Food and Drug Administration (FDA) while evaluating wound related therapeutics. FDA defines complete wound closure as skin re-epithelialization without drainage or dressing requirements confirmed at two consecutive study visits 2 wk apart (11). Keratinocyte migration and proliferation both play a role in covering skin wounds by the process of re-epithelialization. Defects in this function are associated with the clinical phenotype of chronic nonhealing wounds. Ischemia is known to limit re-epithelialization (32, 35, 59). In the current study, ischemic wounds suffered from impaired re-epithelialization. Ischemic conditions clearly compromised the formation of hyperproliferative epithelium. Adult cutaneous tissue repair is accompanied by a robust recruitment of inflammatory cells to the wound site (46). Timely recruitment of macrophages is necessary for wound healing (34, 39). In the nonischemic wounds, macrophage recruitment was rapid, peaking on *day 3* and subsiding on *day 7* postwounding. Such response is consistent with a timely resolution of inflammation. In contrast, macrophage recruitment to the ischemic wound was significantly delayed. Macrophages and their derivatives support angiogenesis (17). Compared with pair-matched nonischemic wounds, the angiogenic response in ischemic wound was clearly blunted. In addition to a lower abundance of endothelial cells, ischemic wounds had fewer organized endothelial cell clusters, which are viewed as a component of the angiogenic response.

Acute response to wounding included differential induction of a specific set of genes on *day 3* in the ischemic wound. This set of 33 genes whose expression was significantly more induced than the response in pair-matched nonischemic wounds was led on a fold-change basis by genes that regulate macrophage, platelet, and nitric oxide biology. Ischemic wounds overexpressed genes encoding neutrophil chemotactic factors. Human alveolar macrophage-derived chemotactic factor (AMCF) for neutrophils amplify the inflammatory processes seen in many acute and chronic diseases (25). CXCL2 or macrophage inflammatory protein 2-alpha (MIP2-α), another chemotactic factor for polymorphonuclear leukocytes, was also overexpressed in ischemic wounds as was CCR1, the

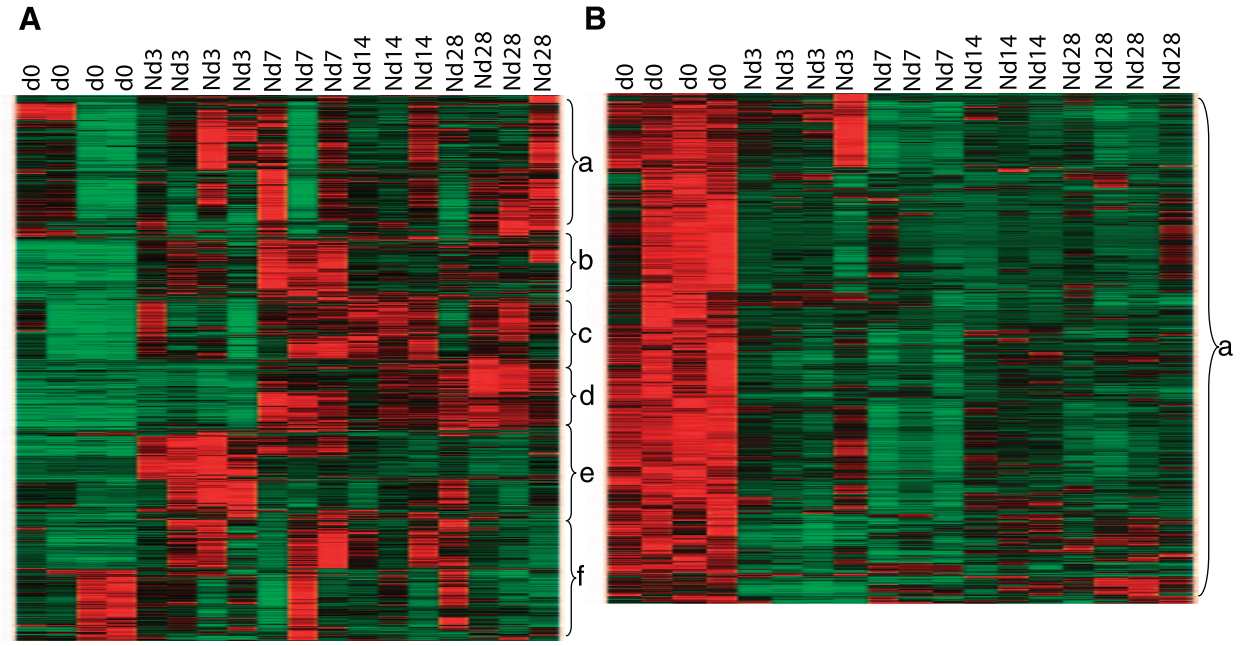


Fig. 8. Heat map illustrating cluster of transcripts that were wound-sensitive in nonischemic wounds. All wound-sensitive transcripts were subjected to hierarchical clustering. *A*: 6 major clusters (*a–f*) of transcripts that were upregulated during the temporal course of healing were identified. *B*: 1 major cluster of genes that was downregulated during the temporal course of healing was also identified. Annotated (according to Affymetrix and Gene Ontology) members of these clusters are listed in Supplemental Table S1. N, nonischemic.

receptor for MIP1-α. While neutrophil influx is an early inflammatory response that is essential for the clearance of bacteria and cellular debris during cutaneous wounding, neutrophil overload at the site of injury is known to adversely influence wound healing. Accelerated wound closure has been shown in neutrophil-depleted mice (9). Inhibition of neutrophil recruitment improves the survival of experimental skin flaps (61). Excessive recruitment of neutrophil to ischemic wound sites is known to take place in other organs (42). In an open wound site such as in the skin, oxidative killing of pathogenic microorganisms represents a major role of infiltrating neutrophils. Thus, an overload of neutrophils at the ischemic wound

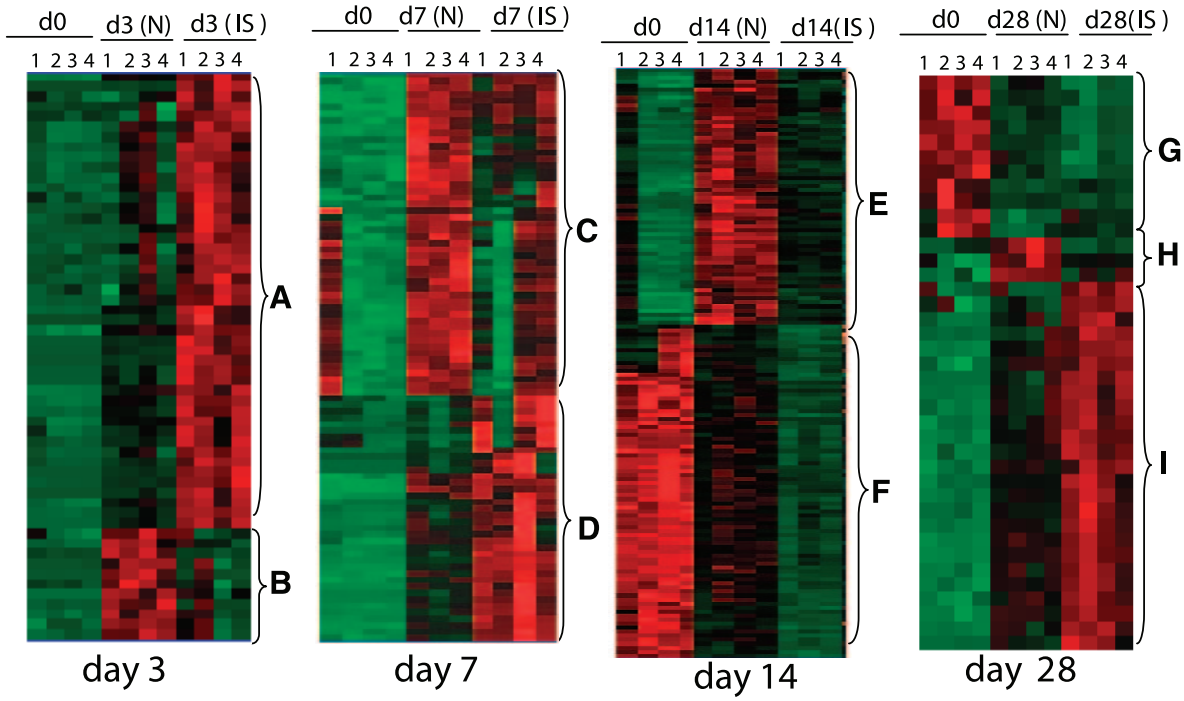


Fig. 9. Heat map illustrating cluster of wound-responsive transcripts that were sensitive to ischemia. All wound-sensitive transcripts were subjected to hierarchical clustering. Nine (*a–i*) major clusters of transcripts were identified over the 4 different time points studied. Annotated (according to Affymetrix and Gene Ontology) members of these clusters are listed in Supplemental Table S3. IS, ischemic.

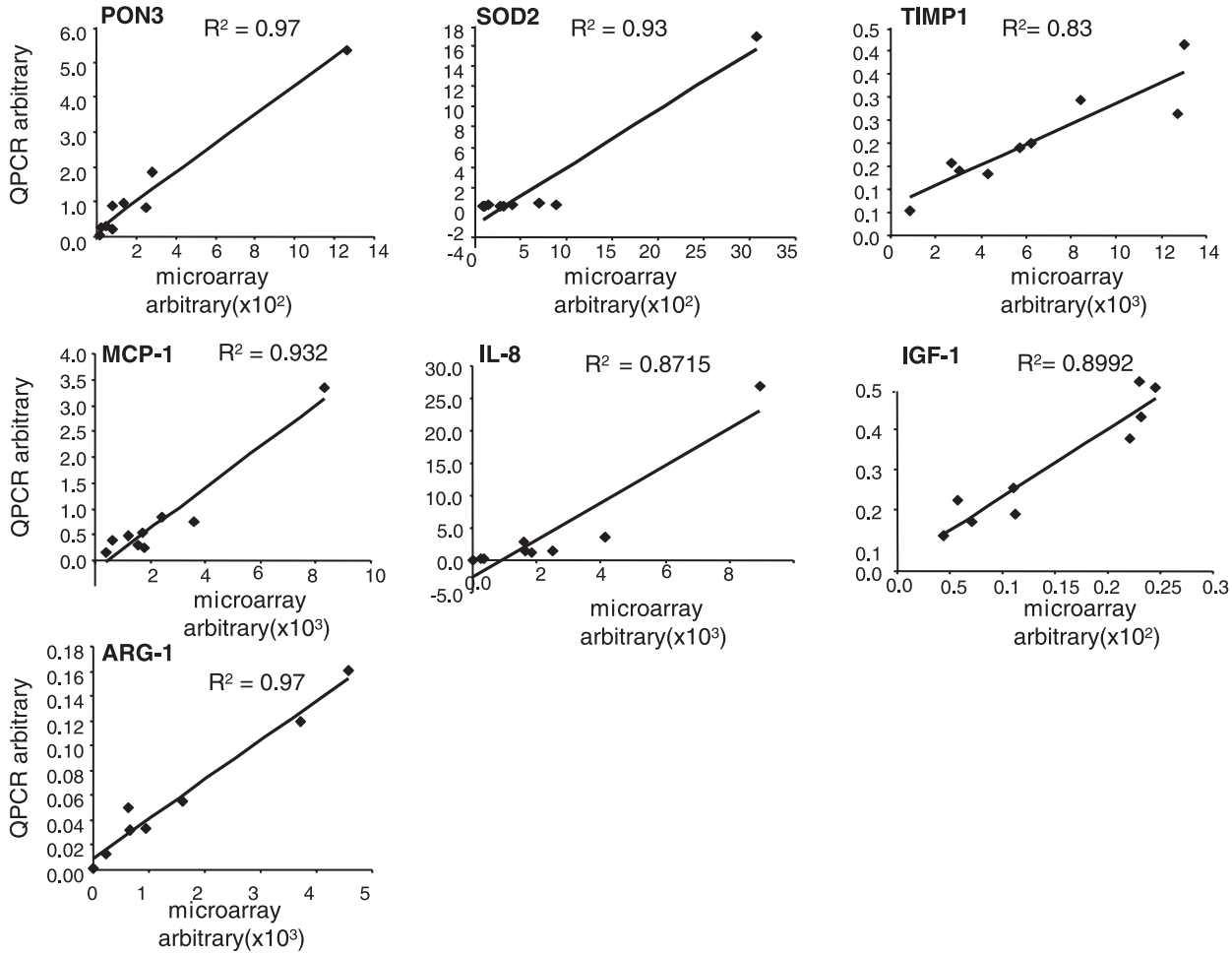


Fig. 10. Validation of ischemia-sensitive candidate genes derived from microarray analyses. Expression levels of selected genes identified using GeneChip analyses were independently determined using real-time quantitative (Q) PCR. Simple regression was used to examine the relationship between QPCR and microarray data. Data obtained from microarray analysis is plotted against QPCR results for each candidate. The regression is derived from the mean of data obtained from ischemic and nonischemic wounds from all 4 time points. All data represent means ± SD ($n$ = 4). IL-8, interleukin-8; IGF-1, insulin-like growth factor-1; PON3, paraoxonase 3; MCP-1, monocyte chemoattractant protein 1; SOD2, superoxide dismutase 2, mitochondrial; TIMP1, matrix metalloproteinase, tissue inhibitor 1; ARG-1, arginase-1.

site is likely to cause oxidative stress (21). Tissue oxidative stress is known to result in the induction of SOD2 or mitochondrial superoxide dismutase as a defense response (65). Indeed, SOD2 was more potently induced in the ischemic wounds.

In the nonischemic wounds, inflammation started subsiding after 7 days of wounding. While macrophage count at the nonischemic wound site started to come down, the count of macrophages in the ischemic wounds was on the rise at this time point. This contrasting feature between the two wound types lays the rationale to hypothesize that wound-induced gene expression would not be the same in the pair-matched ischemic vs. nonischemic wounds. Indeed, two clusters of genes with differential expression profiles were identified. One cluster consisted of genes that were induced in the nonischemic, but not in the ischemic. The second cluster represented a set of genes that were induced in the ischemic but not in the nonischemic wounds. Based on fold-change, this second set of genes was most striking. AMCF, CXCL2, CCR1, and Arg-1 were among the genes that were heavily overexpressed in ischemic wounds. As discussed above, these genes are likely to be involved in overrecruitment of neutrophils and depletion of L-arginine at the wound site, a major substrate for the synthesis of the signaling gas nitric oxide. Consistent with our observations in pigs as well as humans, elevated levels of arginase has been reported in chronic venous ulcer tissues (1).

Two weeks after wounding, when the nonischemic wounds were nearly completely closed, the ischemic wounds had closed less than one-quarter of their initial wound size. Furthermore, this was the time point when closure of the ischemic wounds seemed to stall. Transcriptome analysis of the wound tissue identified two clusters of differential expressed genes. The first cluster consisted of genes that were uniquely induced in the nonischemic wounds. The second cluster was made up of genes, highly expressed in the prewound skin, which were being shut down in response to wounding. The nonischemic wounds expressed a higher abundance of the microtubule-specific protein tubulin-α. Microtubules represent components of the cytoskeleton that play a key role in epithelial migration as well as in wound contraction (3, 38). Overt limitations in both re-epithelialization as well as in overall closure of the ischemic wounds lead to the hypothesis that microtubular assembly and function are limited in cells of the ischemic

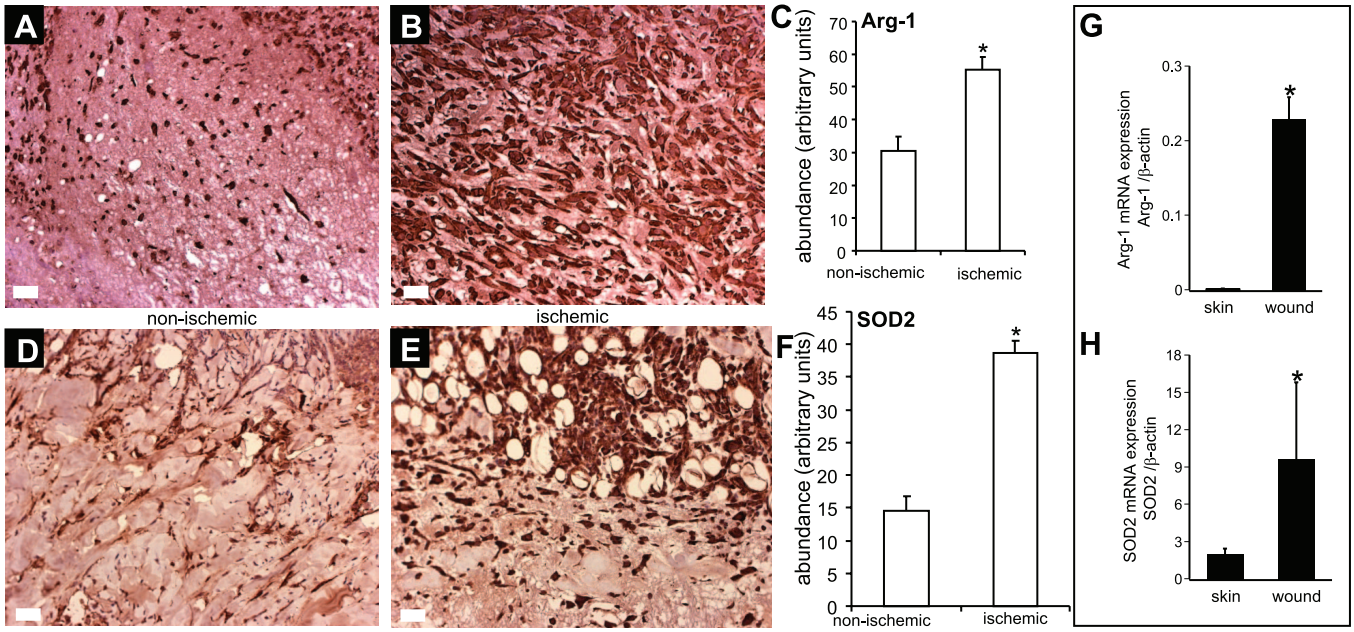


Fig. 11. Immunohistochemical validation of 2 ischemia-sensitive candidate genes Arg-1 and mitochondria superoxide dismutase (SOD2). Wound-edge tissues were collected on *day 3* (SOD2) or *day 7* (Arg-1) after wounding. Formalin-fixed paraffin-embedded biopsy tissues were sectioned (5 μm) and immunostained [diaminobenzidine (DAB) detection with hematoxylin counterstain] with antibodies against either arginase 1 (anti-Arg-1) or SOD2 (anti-SOD2) after heat-induced epitope retrieval. The brown coloration indicates positive staining (*A* and *B*, *D* and *E*). *C, F*: the area of DAB stain was estimated using Adobe Photoshop 6.0 employing a color subtractive process. Data are means ± SD ($n = 3$). *$P < 0.05$. Expression of Arg-1 (*G*) and SOD2 (*H*) in human skin and wound-edge tissue collected from chronic wounds. Quantitative real-time PCR was performed. Data are mean ± SD ($n = 4$). *$P < 0.05$.

wound. Members of the second cluster of genes included adiponectin receptor 2 (ADIPOR2). ADIPOR2 serves as a receptor for globular and full-length adiponectin and triggers peroxisome proliferator-activated receptor (PPAR)-alpha signaling pathways, as well as fatty acid oxidation and glucose uptake by adiponectin. PPAR-α helps resolve skin inflammation (57), and PPAR-α-deficient mice are known to suffer from impaired healing (36). Disruption of ADIPOR abolishes adipo-

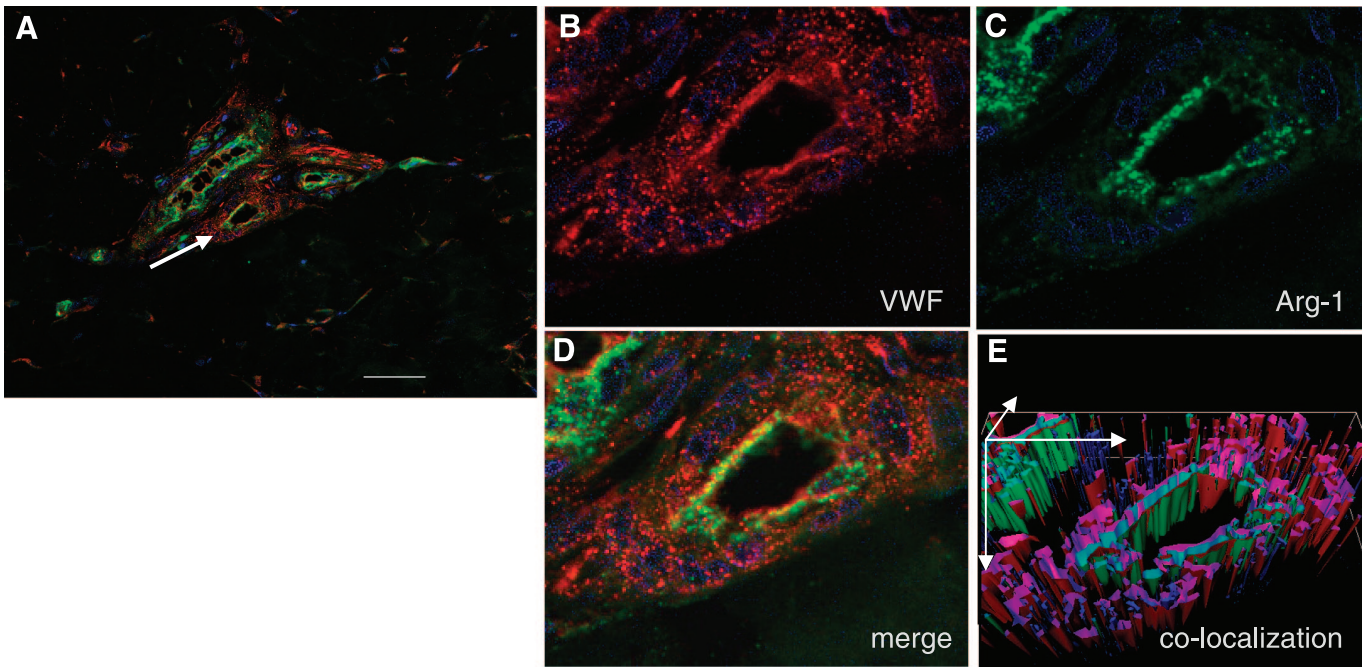


Fig. 12. Localization of arginase-1 in wound vessels. Wound-edge tissues were collected on *day 7* after wounding. OCT-embedded frozen biopsy tissues were sectioned (10 μm) and immunostained simultaneously with antibodies against arginase 1 (anti-arg-1, green) and von Willebrand factor (vWF; endothelial cells, red). *A*: representative immunostained section of a wound showing blood vessels (red) and Arg-1 staining (green). The scale bar = 50 μm. *B*: a zoomed image of VWF-stained (red) blood vessel as shown in *A* with white arrow. *C*: expression of Arg-1 (green). *D*: merged (vWF and Arg-1) image showing colocalization of Arg-1 in VWF-positive areas. *E*: to have a better visualization of the colocalization, the section was also imaged in the *Z*-plane (1 μm increments). The *Z*-images were stacked, and the merged red and green channels were visualized in 3 dimensions using Axiovision Inside4D module (Zeiss).

nectin binding and actions, resulting in increased tissue triglyceride content, inflammation, and oxidative stress, and thus leading to insulin resistance and marked glucose intolerance. ADIPOR2 downregulation is noted in obesity, a condition known to be associated with impaired healing (68). A functionally related gene in this category was hormone-sensitive lipase (LIPE). LIPE is responsible for lipolysis of the subcutaneous fat (44). LIPE expression was markedly lower in the ischemic wounds. Activated by catecholamines, LIPE plays a vital role in the mobilization of free fatty acids from adipose tissue by controlling the rate of lipolysis of the stored triglycerides. LIPE regulates energy homeostasis by catalyzing the rate-limiting step in adipose tissue lipolysis. Genes encoding the bone morphogenetic proteins (BMP) were also downregulated in the ischemic wounds compared with that in the nonischemic wounds. Developmental studies have long implicated the canonical BMP pathway in hair follicle determination and differentiation. Loss of BMP signaling is known to deplete a specific stem cell pool in the skin (31). Genes encoding several proteins of the metallothionein family were also downregulated in the ischemic wounds more than they were in the corresponding nonischemic wounds. Metallothioneins are a class of ubiquitously occurring low-molecular-weight cysteine- and metal-rich proteins that serves to defend the tissue against a variety of stressful conditions. In the skin, metallothioneins are known to play a central role in wound reepithelialization (26).

Four weeks after wounding, the nonischemic wounds were closed, but the ischemic wounds remained less than half closed. Thus, while postclosure remodeling was in progress in the nonischemic wounds, the ischemic wounds were still attempting to re-establish barrier function. This contrast was evident in the transcriptome of tissues taken from the nonischemic and ischemic wounds. The largest cluster of genes that was differentially expressed in this time point was represented by a set of genes that were expressed at a low level on the intact skin. This cluster of genes was heavily overexpressed in the open ischemic wound tissue, while the expression was much lower in the closed nonischemic wounds. Chronic inflammation is commonly associated with ischemic wounds. Overexpression of CCR1 in ischemic wounds is likely to be responsible for chronic inflammation (16). Indeed, the abundance of gp91phox as well as transforming growth factor-β1 in the ischemic wounds is consistent with chronic inflammation. During tooth morphogenesis, epithelial cells differentiate into enamel-secreting ameloblasts. The matrix protein ameloblastin is expressed by differentiating ameloblasts (15). Interestingly, the ischemic wound tissue expressed high levels of aminoblastin. This observation leads to the question whether derailed epithelialization of the ischemic wounds is followed by differentiation of epithelial cells to ameloblasts.

In summary, the current work reports the development and characterization of the first preclinical model of ischemic cutaneous wounds. Proven advantages of the porcine approach to model human cutaneous wounds, a simple surgical approach, and direct functional characterization of the blood flow and tissue oxygenation represent the fundamental strengths of the preclinical model reported herein. Results from the systematic temporal screening of the transcriptome of nonischemic and pair-matched ischemic wounds provide objective rationale toward novel hypotheses that should help elucidate the biology of ischemic cutaneous wounds comprehensively.

## GRANTS

Supported by NIH Grants GM-077185 and GM-069589 and in part by DK-076566 and RR-024384.

## REFERENCES

1. **Abd-El-Aleem SA, Ferguson MW, Appleton I, Kairsingh S, Jude EB, Jones K, McCollum CN, Ireland GW.** Expression of nitric oxide synthase isoforms and arginase in normal human skin and chronic venous leg ulcers. *J Pathol* 191: 434–442, 2000.
2. **Becker F, Raoux MH, Brenot R, David M.** Predictive value of TcPO2 in chronical severe ischemia of lower limbs. *Int J Microcir Clin Exp* 7: 261–271, 1988.
3. **Bement WM, Forscher P, Mooseker MS.** A novel cytoskeletal structure involved in purse string wound closure and cell polarity maintenance. *J Cell Biol* 121: 565–578, 1993.
4. **Bernatchez SF, Parks PJ, Grussing DM, Matalas SL, Nelson GS.** Histological characterization of a delayed wound healing model in pig. *Wound Repair Regen* 6: 223–233, 1998.
5. **Broughton G 2nd, Janis JE, Attinger CE.** The basic science of wound healing. *Plast Reconstr Surg* 117: 12S–34S, 2006.
6. **Cancio LC, Batchinsky AI, Mansfield JR, Panasyuk S, Hetz K, Martini D, Jordan BS, Tracey B, Freeman JE.** Hyperspectral imaging: a new approach to the diagnosis of hemorrhagic shock. *J Trauma* 60: 1087–1095, 2006.
7. **Department of Health and Human Services.** CMS manual system Pub. 100-03 Medicare National Coverage Determinations edited by Services DoHaH: Center for Medicare & Medicaid Services, 2008, http://www.cms.hhs.gov/transmittals/downloads/R83NCD.pdf.
8. **Dor FJ, Gollackner B, Kuwaki K, Ko DS, Cooper DK, Houser SL.** Histopathology of spleen allograft rejection in miniature swine. *Int J Exp Pathol* 86: 57–66, 2005.
9. **Dovi JV, He LK, DiPietro LA.** Accelerated wound closure in neutrophil-depleted mice. *J Leukoc Biol* 73: 448–455, 2003.
10. **Durante W, Johnson FK, Johnson RA.** Arginase: a critical regulator of nitric oxide synthesis and vascular function. *Clin Exp Pharmacol Physiol* 34: 906–911, 2007.
11. **Food and Drug Administration.** Guidance for Industry Chronic Cutaneous Ulcer and Burn Wounds - Developing Products for Treatment, edited by Services USDoHaH: Food and Drug Administration, 2006, http://www.fda.gov/cder/guidance/5512fnl.pdf.
12. **Franzeck UK, Talke P, Bernstein EF, Golbranson FL, Fronek A.** Transcutaneous PO2 measurements in health and peripheral arterial occlusive disease. *Surgery* 91: 156–163, 1982.
13. **Fries RB, Wallace WA, Roy S, Kuppusamy P, Bergdall V, Gordillo GM, Melvin WS, Sen CK.** Dermal excisional wound healing in pigs following treatment with topically applied pure oxygen. *Mutat Res* 579: 172–181, 2005.
14. **Fujihara Y, Koyama H, Ohba M, Tabata Y, Fujihara H, Yonehara Y, Takato T.** Controlled delivery of bFGF to recipient bed enhances the vascularization and viability of an ischemic skin flap. *Wound Repair Regen* 16: 125–131, 2008.
15. **Fukumoto S, Kiba T, Hall B, Iehara N, Nakamura T, Longenecker G, Krebsbach PH, Nanci A, Kulkarni AB, Yamada Y.** Ameloblastin is a cell adhesion molecule required for maintaining the differentiation state of ameloblasts. *J Cell Biol* 167: 973–983, 2004.
16. **Gladue RP, Cole SH, Roach ML, Tylaska LA, Nelson RT, Shepard RM, McNeish JD, Ogborne KT, Neote KS.** The human specific CCR1 antagonist CP-481,715 inhibits cell infiltration and inflammatory responses in human CCR1 transgenic mice. *J Immunol* 176: 3141–3148, 2006.
17. **Gordillo GM, Onat D, Stockinger M, Roy S, Atalay M, Beck FM, Sen CK.** A key angiogenic role of monocyte chemoattractant protein-1 in hemangioendothelioma proliferation. *Am J Physiol Cell Physiol* 287: C866–C873, 2004.
18. **Gould LJ, Leong M, Sonstein J, Wilson S.** Optimization and validation of an ischemic wound model. *Wound Repair Regen* 13: 576–582, 2005.
19. **Greenman RL, Panasyuk S, Wang X, Lyons TE, Dinh T, Longoria L, Giurini JM, Freeman J, Khaodhiar L, Veves A.** Early changes in the skin microcirculation and muscle metabolism of the diabetic foot. *Lancet* 366: 1711–1717, 2005.

20. **Guero SJ, Lacroix PA.** An experimental model of scalp expansion: a method of optimizing flap size and shape. *Plast Reconstr Surg* 87: 776–779, 1991.
21. **Hampton MB, Winterbourn CC.** Redox regulation of neutrophil function. *Antioxid Redox Signal* 4: 1–3, 2002.
22. **Harward TR, Volny J, Golbranson F, Bernstein EF, Fronek A.** Oxygen inhalation–induced transcutaneous PO2 changes as a predictor of amputation level. *J Vasc Surg* 2: 220–227, 1985.
23. **Heinrich W, Lange PM, Stirtz T, Iancu C, Heidemann E.** Isolation and characterization of the large cyanogen bromide peptides from the alpha1- and alpha2-chains of pig skin collagen. *FEBS Lett* 16: 63–67, 1971.
24. **Hetland G, Talgo GJ, Fagerhol MK.** Chemotaxins C5a and fMLP induce release of calprotectin (leucocyte L1 protein) from polymorphonuclear cells in vitro. *Mol Pathol* 51: 143–148, 1998.
25. **Hunninghake GW, Gadek JE, Fales HM, Crystal RG.** Human alveolar macrophage-derived chemotactic factor for neutrophils. Stimuli and partial characterization. *J Clin Invest* 66: 473–483, 1980.
26. **Iwata M, Takebayashi T, Ohta H, Alcalde RE, Itano Y, Matsumura T.** Zinc accumulation and metallothionein gene expression in the proliferating epidermis during wound healing in mouse skin. *Histochem Cell Biol* 112: 283–290, 1999.
27. **Kerrigan CL, Daniel RK.** Critical ischemia time and the failing skin flap. *Plast Reconstr Surg* 69: 986–989, 1982.
28. **Kerrigan CL, Daniel RK.** Skin flap research: a candid view. *Ann Plast Surg* 13: 383–387, 1984.
29. **Khan F, Newton DJ.** Laser Doppler imaging in the investigation of lower limb wounds. *Int J Low Extrem Wounds* 2: 74–86, 2003.
30. **Khaodhiar L, Dinh T, Schomacker KT, Panasyuk SV, Freeman JE, Lew R, Vo T, Panasyuk AA, Lima C, Giurini JM, Lyons TE, Veves A.** The use of medical hyperspectral technology to evaluate microcirculatory changes in diabetic foot ulcers and to predict clinical outcomes. *Diabetes Care* 30: 903–910, 2007.
31. **Kobielak K, Stokes N, de la Cruz J, Polak L, Fuchs E.** Loss of a quiescent niche but not follicle stem cells in the absence of bone morphogenetic protein signaling. *Proc Natl Acad Sci USA* 104: 10063–10068, 2007.
32. **Kopal C, Deveci M, Ozturk S, Sengezer M.** Effects of topical glutathione treatment in rat ischemic wound model. *Ann Plast Surg* 58: 449–455, 2007.
33. **Kuehn BM.** Chronic wound care guidelines issued. *JAMA* 297: 938–939, 2007.
34. **Leor J, Rozen L, Zuloff-Shani A, Feinberg MS, Amsalem Y, Barbash IM, Kachel E, Holbova R, Mardor Y, Daniels D, Ocherashvilli A, Orenstein A, Danon D.** Ex vivo activated human macrophages improve healing, remodeling, and function of the infarcted heart. *Circulation* 114: I94–I100, 2006.
35. **Liechty KW, Nesbit M, Herlyn M, Radu A, Adzick NS, Crombleholme TM.** Adenoviral-mediated overexpression of platelet-derived growth factor-B corrects ischemic impaired wound healing. *J Invest Dermatol* 113: 375–383, 1999.
36. **Michalik L, Desvergne B, Tan NS, Basu-Modak S, Escher P, Rieusset J, Peters JM, Kaya G, Gonzalez FJ, Zakany J, Metzger D, Chambon P, Duboule D, Wahli W.** Impaired skin wound healing in peroxisome proliferator-activated receptor (PPAR)alpha and PPARbeta mutant mice. *J Cell Biol* 154: 799–814, 2001.
37. **Mittermayr R, Morton T, Hofmann M, Helgerson S, van Griensven M, Redl H.** Sustained (rh)VEGF(165) release from a sprayed fibrin biomatrix induces angiogenesis, up-regulation of endogenous VEGF-R2, and reduces ischemic flap necrosis. *Wound Repair Regen* 16: 542–550, 2008.
38. **Omelchenko T, Vasiliev JM, Gelfand IM, Feder HH, Bonder EM.** Rho-dependent formation of epithelial "leader" cells during wound healing. *Proc Natl Acad Sci USA* 100: 10788–10793, 2003.
39. **Orenstein A, Kachel E, Zuloff-Shani A, Paz Y, Sarig O, Haik J, Smolinsky AK, Mohr R, Shinar E, Danon D.** Treatment of deep sternal wound infections post-open heart surgery by application of activated macrophage suspension. *Wound Repair Regen* 13: 237–242, 2005.
40. **Perez R, Davis SC.** Relevance of animal models for wound healing. *Wounds* 20: 3–8, 2008.
41. **Powell RJ, Simons M, Mendelsohn FO, Daniel G, Henry TD, Koga M, Morishita R, Annex BH.** Results of a double-blind, placebo-controlled study to assess the safety of intramuscular injection of hepatocyte growth factor plasmid to improve limb perfusion in patients with critical limb ischemia. *Circulation* 118: 58–65, 2008.
42. **Price CJ, Menon DK, Peters AM, Ballinger JR, Barber RW, Balan KK, Lynch A, Xuereb JH, Fryer T, Guadagno JV, Warburton EA.** Cerebral neutrophil recruitment, histology, and outcome in acute ischemic stroke: an imaging-based study. *Stroke* 35: 1659–1664, 2004.
43. **Quirinia A.** Ischemic wound healing and possible treatments. *Drugs Today (Barc)* 36: 41–53, 2000.
44. **Reynisdottir S, Dauzats M, Thorne A, Langin D.** Comparison of hormone-sensitive lipase activity in visceral and subcutaneous human adipose tissue. *J Clin Endocrinol Metab* 82: 4162–4166, 1997.
45. **Roy S, Khanna S, Kuhn DE, Rink C, Williams WT, Zweier JL, Sen CK.** Transcriptome analysis of the ischemia-reperfused remodeling myocardium: temporal changes in inflammation and extracellular matrix. *Physiol Genomics* 25: 364–374, 2006.
46. **Roy S, Khanna S, Rink C, Biswas S, Sen CK.** Characterization of the acute temporal changes in excisional murine cutaneous wound inflammation by screening of the wound-edge transcriptome. *Physiol Genomics* 34: 162–184, 2008.
47. **Roy S, Khanna S, Shah H, Rink C, Phillips C, Preuss H, Subbaraju GV, Trimurtulu G, Krishnaraju AV, Bagchi M, Bagchi D, Sen CK.** Human genome screen to identify the genetic basis of the anti-inflammatory effects of Boswellia in microvascular endothelial cells. *DNA Cell Biol* 24: 244–255, 2005.
48. **Roy S, Khanna S, Wallace WA, Lappalainen J, Rink C, Cardounel AJ, Zweier JL, Sen CK.** Characterization of perceived hyperoxia in isolated primary cardiac fibroblasts and in the reoxygenated heart. *J Biol Chem* 278: 47129–47135, 2003.
49. **Roy S, Khanna S, Yeh PE, Rink C, Malarkey WB, Kiecolt-Glaser J, Laskowski B, Glaser R, Sen CK.** Wound site neutrophil transcriptome in response to psychological stress in young men. *Gene Expression* 12: 273–287, 2005.
50. **Roy S, Patel D, Khanna S, Gordillo GM, Biswas S, Friedman A, Sen CK.** Transcriptome-wide analysis of blood vessels laser captured from human skin and chronic wound-edge tissue. *Proc Natl Acad Sci USA* 104: 14472–14477, 2007.
51. **Sen CK.** Wound healing essentials: let there be oxygen. *Wound Repair Regen* 17: 1–18, 2009.
52. **Sen CK, Khanna S, Babior BM, Hunt TK, Ellison EC, Roy S.** Oxidant-induced vascular endothelial growth factor expression in human keratinocytes and cutaneous wound healing. *J Biol Chem* 277: 33284–33290, 2002.
53. **Shimazaki M, Matsuki T, Yamauchi K, Iwata M, Takahashi H, Genda S, Ohata J, Nakamura Y, Inaba Y, Yokouchi S, Kikuiri T, Ashie T.** Assessment of lower limb ischemia with measurement of skin perfusion pressure in patients on hemodialysis. *Ther Apher Dial* 11: 196–201, 2007.
54. **Singer AJ, McClain SA.** Development of a porcine excisional wound model. *Acad Emerg Med* 10: 1029–1033, 2003.
55. **Slovut DP, Sullivan TM.** Critical limb ischemia: medical and surgical management. *Vasc Med* 13: 281–291, 2008.
56. **Sorg BS, Moeller BJ, Donovan O, Cao Y, Dewhirst MW.** Hyperspectral imaging of hemoglobin saturation in tumor microvasculature and tumor hypoxia development. *J Biomed Opt* 10: 44004, 2005.
57. **Staumont-Salle D, Abboud G, Brenuchon C, Kanda A, Roumier T, Lavogiez C, Fleury S, Remy P, Papin JP, Bertrand-Michel J, Terce F, Staels B, Delaporte E, Capron M, Dombrowicz D.** Peroxisome proliferator-activated receptor alpha regulates skin inflammation and humoral response in atopic dermatitis. *J Allergy Clin Immunol* 121: 962–968, 2008.
58. **Sullivan TP, Eaglstein WH, Davis SC, Mertz P.** The pig as a model for human wound healing. *Wound Repair Regen* 9: 66–76, 2001.
59. **Sun W, Lin H, Xie H, Chen B, Zhao W, Han Q, Zhao Y, Xiao Z, Dai J.** Collagen membranes loaded with collagen-binding human PDGF-BB accelerate wound healing in a rabbit dermal ischemic ulcer model. *Growth Factors* 25: 309–318, 2007.
60. **Tanaka R, Wada M, Kwon SM, Masuda H, Carr J, Ito R, Miyasaka M, Warren SM, Asahara T, Tepper OM.** The effects of flap ischemia on normal and diabetic progenitor cell function. *Plast Reconstr Surg* 121: 1929–1942, 2008.
61. **Torkvist L, Mansson P, Raud J, Larsson J, Thorlacius H.** Role of CD18-dependent neutrophil recruitment in skin and intestinal wound healing. *Eur Surg Res* 33: 249–254, 2001.
62. **Underwood RA, Gibran NS, Muffley LA, Usui ML, Olerud JE.** Color subtractive-computer-assisted image analysis for quantification of cutane-

ous nerves in a diabetic mouse model. *J Histochem Cytochem* 49: 1285–1291, 2001.

63. **Wang JF, Olson ME, Reno CR, Kulyk W, Wright JB, Hart DA.** Molecular and cell biology of skin wound healing in a pig model. *Connect Tissue Res* 41: 195–211, 2000.
64. **Wang JF, Olson ME, Reno CR, Wright JB, Hart DA.** The pig as a model for excisional skin wound healing: characterization of the molecular and cellular biology, and bacteriology of the healing process. *Comp Med* 51: 341–348, 2001.
65. **Whittaker JW.** The irony of manganese superoxide dismutase. *Biochem Soc Trans* 31: 1318–1321, 2003.
66. **Wong GH, Elwell JH, Oberley LW, Goeddel DV.** Manganous superoxide dismutase is essential for cellular resistance to cytotoxicity of tumor necrosis factor. *Cell* 58: 923–931, 1989.
67. **Yamada T, Ohta T, Ishibashi H, Sugimoto I, Iwata H, Takahashi M, Kawanishi J.** Clinical reliability and utility of skin perfusion pressure measurement in ischemic limbs–comparison with other noninvasive diagnostic methods. *J Vasc Surg* 47: 318–323, 2008.
68. **Yamauchi T, Nio Y, Maki T, Kobayashi M, Takazawa T, Iwabu M, Okada-Iwabu M, Kawamoto S, Kubota N, Kubota T, Ito Y, Kamon J, Tsuchida A, Kumagai K, Kozono H, Hada Y, Ogata H, Tokuyama K, Tsunoda M, Ide T, Murakami K, Awazawa M, Takamoto I, Froguel P, Hara K, Tobe K, Nagai R, Ueki K, Kadowaki T.** Targeted disruption of AdipoR1 and AdipoR2 causes abrogation of adiponectin binding and metabolic actions. *Nat Med* 13: 332–339, 2007.
69. **Yang Z, Ming XF.** Endothelial arginase: a new target in atherosclerosis. *Curr Hypertens Rep* 8: 54–59, 2006.